# *Chandra* unveils a binary active galactic nucleus in Mrk 463

Stefano Bianchi,[1][*] Marco Chiaberge,[2] Enrico Piconcelli,[3] Matteo Guainazzi[4] and Giorgio Matt[1]

[1]*Dipartimento di Fisica, Università degli Studi Roma Tre, via della Vasca Navale 84, 00146 Roma, Italy*
[2]*Space Telescope Science Institute, 3700 San Martin Drive, Baltimore, MD 21218*
[3]*Osservatorio Astronomico di Roma (INAF), Via Frascati 33, I-00040 Monte Porzio Catone, Italy*
[4]*XMM–Newton Science Operations Centre, European Space Astronomy Centre, ESA, Apartado 50727, E-28080 Madrid, Spain*

**ABSTRACT**

We analyse *Chandra*, *XMM–Newton* and *Hubble Space Telescope* (*HST*) data of the double-nucleus Ultraluminous Infrared Galaxy (ULIRG), Mrk 463. The *Chandra* detection of two luminous ($L_{2-10\,\mathrm{keV}} = 1.5 \times 10^{43}$ and $3.8 \times 10^{42}$ erg cm$^{-2}$ s$^{-1}$), unresolved nuclei in Mrk 463 indicates that this galaxy hosts a binary active galactic nucleus (AGN), with a projected separation of $\simeq$3.8 kpc ($3.83 \pm 0.01$ arcsec). While the East nucleus was already known to be a type 2 Seyfert (and this is confirmed by our *Chandra* detection of a neutral iron line), this is the first unambiguous evidence in favour of the AGN nature of the West nucleus. Mrk 463 is therefore the clearest case so far for a binary AGN, after NGC 6240.

**Key words:** galaxies: active – galaxies: Seyfert – X-rays: individual: Mrk 463 – X-rays: individual: Mrk 463E – X-rays: individual: Mrk 463W.

## 1 INTRODUCTION

If, as commonly believed, galaxies merge hierarchically and all galactic bulges contain supermassive black holes (BHs), the formation of binary/multiple BHs should be therefore inevitable (e.g. Milosavljević & Merritt 2001; Haiman & Quataert 2004). Interestingly, the presence of binary supermassive BHs has been also invoked to account for many important aspects of the active galactic nuclei (AGN) phenomenon (see Komossa 2003, for a review), i.e. the formation of the molecular torus (key ingredient of the Unified models), the difference between radio-loud and radio-quiet AGN, the distortions and the bendings in radio jets, and the random orientations of the radio jets and biconical narrow-line regions (NLRs) with respect to the rotational axes of the host galaxy disc. Furthermore, coalescing binary BHs are expected to be the most powerful sources of gravitational waves.

However, an observational evidence for binary BHs is so far very rare. The first clear-cut example was found in the Ultraluminous Infrared Galaxy (ULIRG: Sanders & Mirabel 1996), NGC 6240 (Komossa et al. 2003). The active nature of the two nuclei is unambiguous and their projected distance ($\simeq$1 kpc) remains the shortest measured so far for such a system. A second, close binary AGN ($\simeq$4.6 kpc) was later claimed in Arp 299 (Ballo et al. 2004). A system with a larger projected distance between the nuclei ($\simeq$10.5 kpc) was then found in the galactic pair ESO 509$-$IG066 (Guainazzi et al. 2005b). Finally, Evans et al. (2007) revealed the AGN nature

of the companion of the Fanaroff–Riley type II (FR II) radio source 3C 321.

Mrk 463 ($z = 0.0504$) is an ULIRG with a double nucleus, Mrk 463W and Mrk 463E, and tidal tails due to a recent merger between two spiral galaxies (Mazzarella et al. 1991, and references therein). The Eastern nucleus is commonly classified as a type 2 Seyfert (e.g. Shuder & Osterbrock 1981; Hutchings & Neff 1989), with broad optical lines detected in polarized light (Miller & Goodrich 1990). On the other hand, the nature of the Western nucleus is ambiguous: a type 2 Seyfert, a low-ionization nuclear emission-line region (LINER) or a powerful starbust galaxy is all possible (e.g. Shuder & Osterbrock 1981; Mazzarella et al. 1991). In the X-rays, Mrk 463 was not detected by *Ginga* ($L_{2-10\,\mathrm{keV}} < 2 \times 10^{43}$ erg s$^{-1}$: Awaki & Koyama 1993), but it was detected in the soft X-rays by *Einstein* and *ROSAT* (Polletta et al. 1996). *ASCA* revealed a very absorbed spectrum (Ueno et al. 1996), confirmed by *BeppoSAX*, together with the detection of a strong iron line (Landi & Bassani 2001). These results were further refined by the *XMM–Newton* observation (Imanishi & Terashima 2004).

In this paper, we present a *Chandra* observation of Mrk 463, where the two nuclei are spatially resolved for the first time in the X-rays, performing a detailed comparison with *Hubble Space Telescope* (*HST*) optical and near-infrared (NIR) data.

## 2 OBSERVATIONS AND DATA REDUCTION

In the following, errors correspond to the 90 per cent confidence level for one interesting parameter ($\Delta\chi^2 = 2.71$), where not otherwise stated. The adopted cosmological parameters are

[*]E-mail: bianchi@fis.uniroma3.it

$H_0 = 70$ km s$^{-1}$ Mpc$^{-1}$, $\Omega_\Lambda = 0.73$ and $\Omega_m = 0.27$ (i.e. the default ones in XSPEC 12.3.1: Arnaud 1996). At the distance of Mrk 463, 1 arcsec corresponds to 986 pc. In all the fits, the Galactic column density along the line of sight to Mrk 463 is included ($2.06 \times 10^{20}$ cm$^{-2}$: Dickey & Lockman 1990).

### 2.1 X-rays: *Chandra* and *XMM–Newton*

Mrk 463 was observed by *Chandra* on 2004, June 11 (obsid 4913), with the Advanced CCD Imaging Spectrometer (ACIS: Garmire et al. 2003). Data were reduced with the Chandra Interactive Analysis of Observations (CIAO: Fruscione et al. 2006) 3.4 and the Chandra Calibration Data Base (CALDB) 3.4.1 software, adopting standard procedures, for a final net exposure time of about 49 ks. Images were corrected for known aspect offsets, reaching a nominal astrometric accuracy of 0.6 arcsec (at the 90 per cent confidence level). Three extraction regions were used for the *Chandra* data: two circular regions with radius of 2 arcsec centred at the hard X-ray nuclei and a circular region with radius of 7 arcsec, encompassing all the soft X-ray extended emission, but excluding the two previous regions. Spectra were rebinned to have at least 25 counts in each bin, in order to use the $\chi^2$ statistics. Local fits were also performed in the 5.5–7.0 keV energy range with the unbinned spectra, using the Cash (1976) statistics, in order to better assess the presence of the iron lines and measure their properties. We refer the reader to Guainazzi, Matt & Perola (2005a) for details on this kind of analysis.

Mrk 463 was observed by *XMM–Newton* on 2001, December 22 (obsid 0094401201), with the EPIC CCD cameras, the pn (Strüder et al. 2001) and two MOS (Turner et al. 2001), operated in full frame and medium filter. These data were already presented by Imanishi & Terashima (2004), but we reduced them with the latest software and calibration files in order to do a better comparison with the *Chandra* spectrum. Source extraction radii and screening for intervals of flaring particle background were performed with SAS 7.1.0 (Gabriel et al. 2004) via an iterative process which leads to a maximization of the signal-to-noise ratio (SNR), similarly to what described in Piconcelli et al. (2004). After this process, the net exposure time was of about 21, 25 and 26 ks for pn, MOS1 and MOS2, respectively, adopting extraction radii of 28 arcsec for all the cameras.

The background spectra were extracted from source-free circular regions with a radius of 50 arcsec. Pattern 0 to 4 were used for the pn spectrum, while MOS spectra include patterns 0 to 12. Spectra were binned in order to oversample the instrumental resolution by at least a factor of 3 and to have no less than 30 counts in each background-subtracted spectral channel.

### 2.2 Optical and NIR: *HST*

*HST* observations were retrieved from the Multimission Archive at STScI and processed through the standard on-the-fly reprocessing system. Mrk 463 was observed with WFPC2, NICMOS and with various optical and NIR filters, as a part of different observational programmes. We use NIR observations with NICMOS-NIC2 (NIR filters F110W, F160W, F207M) from programme GO 7213. We also use optical observations with WFPC2 from programme GO 5982 (*F*814*W* filter), GO 6301 (F588N and FR533N filters). The images from GO 6301 are combined to remove cosmic rays using the task CRREJ in IRAF, and bad columns were removed using FIXPIX. For the *F*814*W* filter (left-hand panel of Fig. 1), only one exposure was taken. Therefore, in order to remove cosmic rays and hot pixels, we run an iterative process using the tasks COSMICRAYS and FIXPIX to identify cosmic rays and hot pixels and then 'fix' the image.

The image taken with the ramp filter FR533N is centred at the redshifted wavelength of the [O III]$\lambda$5007 Å emission line, while the F588N filter only includes the nearby continuum emission. The image with F588N is then rescaled to match the continuum emission detected with the FR533N filter, and the continuum emission is subtracted in order to obtain a 'pure' [O III] image (Fig. 2).

We measure the NIR flux of the nuclei from the NICMOS images by performing aperture photometry using the task RADPROF. The aperture radius is set at ∼6 pixel from the point spread function (PSF) centre (corresponding to ∼0.45 arcsec) for the brightest sources (e.g. E nucleus in F207M), and closer to the centre (∼4 pixel) for the faintest (e.g. W nucleus in F110W). The background was measured in an annulus of 1 pixel width, as close as possible to the nucleus, just outside the aperture radius. Errors on the measurements depend on the contrast between the brightness of the nucleus and the surrounding background. We estimate that
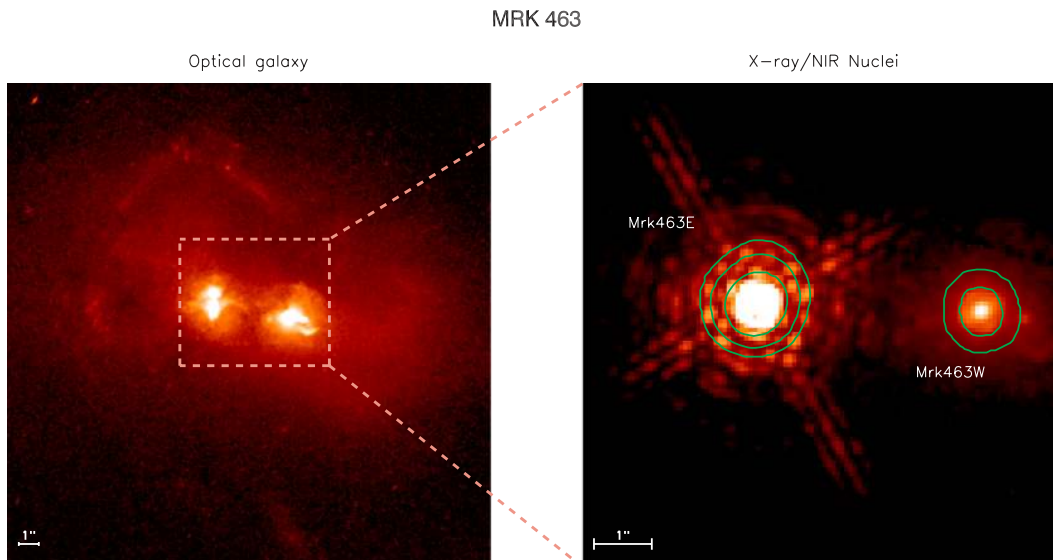


**Figure 1.** Mrk 463 (north is up, east to the left). Left-hand panel: *HST* optical (*F*814*W* filter) image of this double-nucleus galaxy. Right-hand panel: hard X-rays *Chandra* contours superimposed on the 2.1-μm *HST* image: two unresolved nuclei are clearly detected in both the bands.
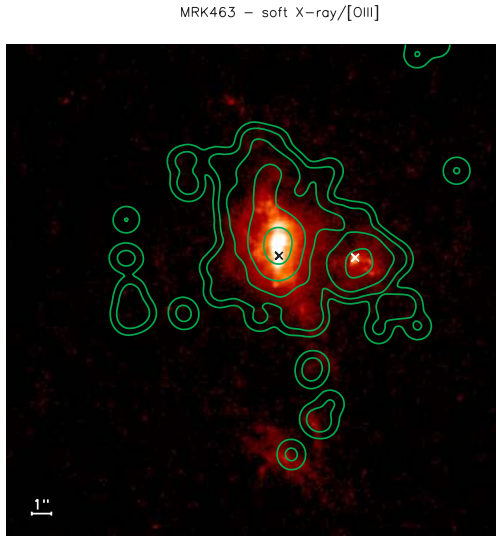
MRK463 − soft X−ray/[OIII]



**Figure 2.** Mrk 463: soft X-rays *Chandra* contours superimposed on the *HST* [O III] emission. The two crosses show the positions of the nuclei (see Fig. 1). North is up, east to the left.

errors are of the order of 5 per cent (corresponding to the NICMOS photometric calibration error) for the brightest sources and up to 40 per cent for the W nucleus in F110W. We convert the counts measured inside the aperture into total counts of the PSF using aperture corrections derived by performing similar aperture photometry on

appropriate synthetic PSFs obtained with the TINYTIM software. The counts are then converted into physical units using the PHOTFLAM keyword in the image header as a first-order approximation. The PHOTFLAM keyword assumes a source with a flat-continuum slope ($F_\lambda \propto \lambda^\beta$, with $\beta = 0$). Thus, in presence of steep spectral slopes, the conversion may be incorrect. By using the task BANDPAR in SYNPHOT, we iteratively derive the slope of the nuclei, and recalculate the value of PHOTFLAM corresponding to the measured slope,

The NIR filters on *HST*/NICMOS are similar but not equivalent to the standard *J*, *H* and *K* filters used in ground-based telescopes (Barker et al. 2007). In order to compare our measurements with *K*-band magnitudes published in the literature, we measure the flux of the nuclei in the NICMOS F207M image, inside an aperture of 1 arcsec radius (corresponding to 13.25 pixel). In this case, the background is measured far away from the nuclei at a distance of ∼6 arcsec. We then convert the fluxes measured from the *HST* image to *K*-band magnitudes using the task CALCPHOT in SYNPHOT. The observations were performed before the cryo-cooler installation on NICMOS, therefore we modify the default settings of the task to make the use of the correct system throughput tables for the time of the observations.

## 3 IMAGING ANALYSIS

The high-energy (>2 keV) *Chandra* image of Mrk 463 clearly shows the presence of two bright, unresolved nuclei. Their positions are coincident with the two nuclei detected in the *HST* NIR image (Fig. 1): Mrk 463E ($K = 10.98 \pm 0.05$ mag) and Mrk 463W ($K = 13.63 \pm$
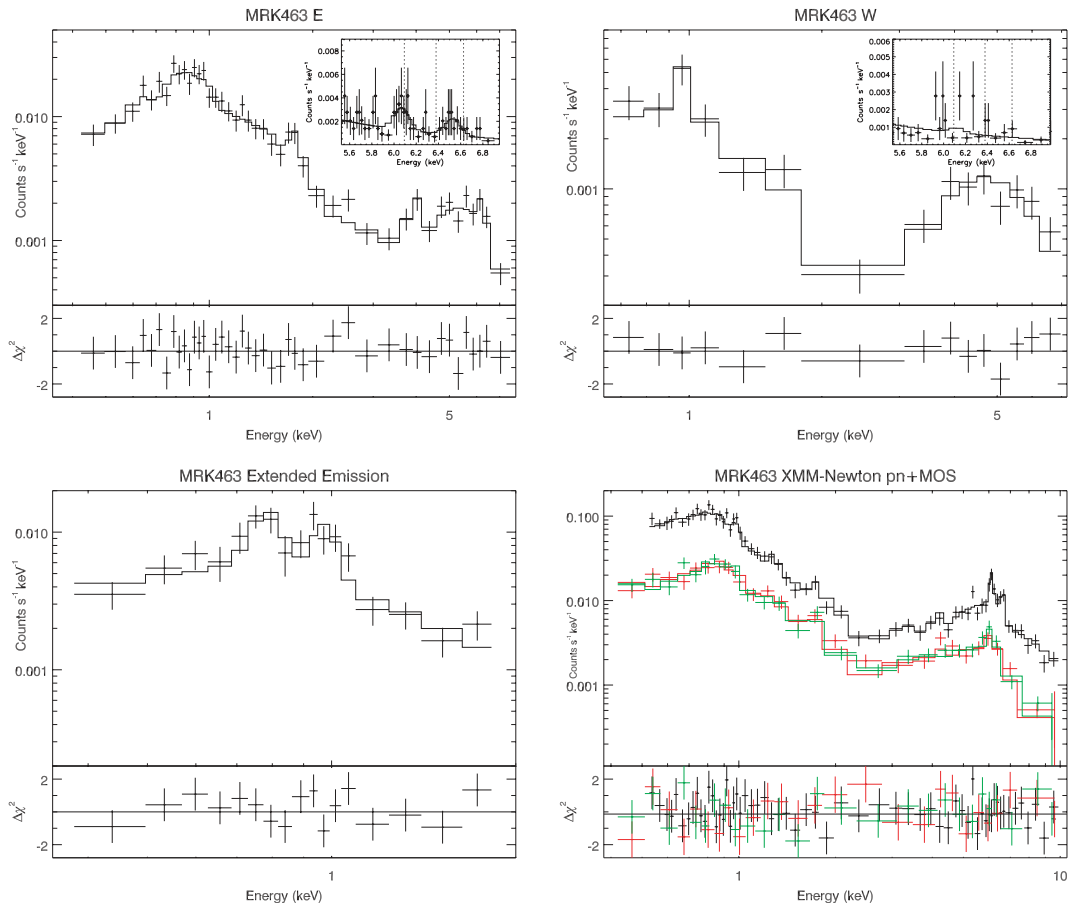


**Figure 3.** *Chandra* spectra of Mrk 463E, Mrk 463W and the extended emission. See the text for details. *XMM–Newton* EPIC, MOS1 and MOS2 spectra of Mrk 463.

**Table 1.** Best-fitting parameters for the *Chandra* and *XMM–Newton* spectra analysed in this paper. Fluxes are in units of $10^{-13}$ erg cm$^{-2}$ s$^{-1}$, luminosities in units of $10^{42}$ erg s$^{-1}$, emission-line fluxes in units of $10^{-6}$ ph cm$^{-2}$ s$^{-1}$. In the fits, only significant (at the 90 per cent level) emission lines were added and, once identified, their centroid energies were fixed to the theoretical values. For the He-like triplets, we fixed an average centroid energy between the three components (r), (i) and (f). Values followed by * were extracted from local fits in the 5.5–7 keV band, with the continuum modelled as an absorbed power law, with photon index and column density fixed to the best-fitting values in the broad-band fit. See the text for details.

| | Chandra | | | XMM–Newton |
| --- | --- | --- | --- | --- |
| | Mrk 463E | Mrk 463W | Extended | Mrk 463E+W |
| $N_{\mathrm{H},1}$ ($10^{22}$ cm$^{-2}$) | $0.09 \pm 0.07$ | $<0.15$ | $<0.11$ | $<0.03$ |
| $N_{\mathrm{H},2}$ ($10^{22}$ cm$^{-2}$) | $71^{+18}_{-15}$ | $32^{+9}_{-6}$ | – | $55^{+10}_{-7}$ |
| $\Gamma$ | $2.3^{+0.3}_{-0.2}$ | $2.2 \pm 0.2$ | $2.3 \pm 0.3$ | $2.04^{+0.09}_{-0.11}$ |
| $F_{6.4}$ | $6.2^{+4.4}_{-3.6}{}^{*}$ | $< 2.0$ | – | $9.4^{+3.1}_{-2.7}$ |
| EW$_{6.4}$ (eV) | $210^{+150}_{-120}{}^{*}$ | $<260^{*}$ | – | $280 \pm 90$ |
| $\chi^2$/dof | 25/29 | 9/10 | 13/12 | 76/94 |
| $F_{0.5-2}$ | $0.5 \pm 0.1$ | $0.11 \pm 0.04$ | $0.21 \pm 0.04$ | $1.1 \pm 0.1$ |
| $F_{2-10}$ | $4.1 \pm 1.8$ | $1.8 \pm 0.8$ | – | $6.9 \pm 2.0$ |
| $L_{2-10}$ | $15 \pm 7$ | $3.8 \pm 1.7$ | – | $23 \pm 7$ |
| Fluxes of other emission lines | | | | |
| O VII Kα (rif) (0.568 keV) | – | – | – | $8.7^{+0.5}_{-0.7}$ |
| O VIII Kα (0.654 keV) | $3.5^{+5.5}_{-3.4}$ | – | – | $4.8^{+2.1}_{-3.0}$ |
| O VII RRC (0.739 keV) | – | – | – | $6.0^{+1.7}_{-2.4}$ |
| Fe XVII 3d-2p (0.826 keV) | $3.5^{+2.3}_{-2.0}$ | – | $3.1^{+1.2}_{-1.0}$ | $7.2^{+1.6}_{-1.9}$ |
| Ne IX Kα (rif) (0.914 keV) | $3.1^{+1.7}_{-1.6}$ | – | – | $7.3^{+1.4}_{-1.6}$ |
| Ne X Kα (1.022 keV) | $2.0 \pm 1.1$ | $0.9 \pm 0.6$ | $1.7 \pm 0.6$ | $5.7^{+1.1}_{-1.3}$ |
| Ne X Kβ (1.211 keV) | – | – | – | $1.3^{+0.8}_{-0.9}$ |
| Mg XI Kα (rif) (1.342 keV) | – | – | – | $1.4 \pm 0.7$ |
| Si XIII Kα (rif) (1.853 keV) | $0.5 \pm 0.4$ | – | – | $0.7^{+0.6}_{-0.5}$ |
| Ar XVII Kα (rif) (3.123 keV) | – | – | – | $1.1^{+0.7}_{-0.6}$ |
| Ar XVII Kβ (3.680 keV) | – | – | – | $1.7 \pm 0.7$ |
| Ca XX Kα (4.070 keV) | $1.2 \pm 0.6$ | – | – | – |
| Unid. ($4.31 \pm 0.04$ keV) | – | – | – | $1.6^{+0.9}_{-0.8}$ |
| Fe XXVI (6.96 keV) | $1.6^{+1.3}_{-0.9}{}^{*}$ | – | – | $3.4 \pm 2.3$ |

0.06 mag), separated by $3.83 \pm 0.01$ arcsec. The soft X-ray ($<2$ keV) *Chandra* image still presents two nuclei and some extended emission, which seems more clearly related to the brightest Mrk 463E. The shape of the soft X-ray emission closely resembles the NLR, mapped by the [O III] emission (Fig. 2). This is a very common property of type 2 Seyfert galaxies and suggests a common origin in a gas photoionized by the AGN emission (see e.g. Bianchi, Guainazzi & Chiaberge 2006).

## 4 SPECTRAL ANALYSIS

The *Chandra* spectra of the two nuclei are typical of Compton-thin type 2 Seyfert galaxies: they are strongly absorbed, with a soft excess component in the low-energy band (see upper panels of Fig. 3). They are well fitted by two power laws with the same photon index, one of which absorbed by a column density of a few $10^{23}$ cm$^{-2}$. A number of strong emission lines are also required for the east spectrum, while only emission from Ne X Kα is detected in the west spectrum, which has a poorer SNR (see Table 1). Interestingly, the soft excess in source E is further absorbed by a local column density of the order of $10^{21}$ cm$^{-2}$, even if with large uncertainty. The spectrum of the extended emission (which excludes the nuclei) is fully consistent with the soft X-ray emission from the nuclei, being well fitted by a

simple power law and a couple of emission lines (see lower left-hand panel of Fig. 3 and Table 1).

The 2–10 keV absorption-corrected luminosities strongly indicate that both nuclei are AGN, being $1.5 \times 10^{43}$ and $3.8 \times 10^{42}$ erg s$^{-1}$, much larger than observed in Starburst galaxies and LINERs (e.g. $\langle L_{\mathrm{x}}^{\mathrm{SB}} \rangle = 8.5 \times 10^{39}$ and $\langle L_{\mathrm{x}}^{\mathrm{L}} \rangle = 1.7 \times 10^{40}$ erg s$^{-1}$: González-Martín et al. 2006). In addition, the presence of a strong iron line [equivalent width (EW) $\simeq 250$ eV] is clearly detected in the local fit of the brightest nucleus, while the upper limit found for the other source is largely consistent with what expected for an AGN (see Table 1).

The *XMM–Newton* spectrum comprises the sum of the two nuclei and the extended emission. Indeed, the best fit is what expected from a Compton-thin type 2 Seyfert, with a strong Fe Kα line at high energies and several emission lines from lighter metals in the soft X-rays. The column density of the absorber is intermediate between the two measured separately for the two nuclei with *Chandra*. The 0.5–2 and 2–10 keV fluxes are consistent, within errors, with the sum of all the contributions measured with *Chandra*. The neutral iron-line flux is larger than the one observed for nucleus east, suggesting the intriguing possibility that the remaining flux comes from an otherwise undetected iron-line flux in nucleus west. However, the first two fluxes are consistent within errors and so nothing conclusive can be said in this respect.
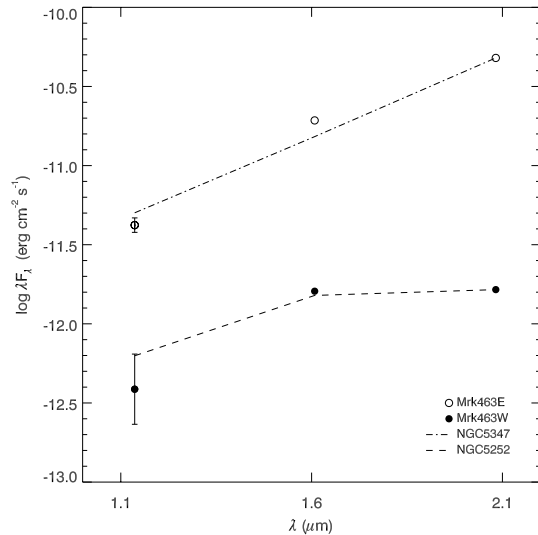
**Figure 4.** The *HST* NIR spectrum of the two nuclei in Mrk 463. In comparison, the *HST* NIR spectrum of type 2 Seyfert galaxies is plotted, renormalized at the 2.1-μm flux of the nuclei. See the text for details.

As found in the *Chandra* data, the soft X-ray emission is dominated by a wealth of emission lines from ionized metals. The much better quality of the *XMM–Newton* data allows us to detect the O VII Radiative Recombination Continuum (RRC), a clear signature of photoionization (see e.g. Guainazzi & Bianchi 2007, and references therein). Finally, a strong Fe XXVI line is detected (as already reported by Imanishi & Terashima 2004), confirming the one observed in the *Chandra* east nucleus (although, in the latter case, the centroid energy is marginally inconsistent with 6.96 keV and may be blended with Fe XXV). Emission lines from ionized iron are common in type 2 Seyfert galaxies and may originate in a more ionized phase of the circumnuclear gas photoionized by the nuclear continuum (see e.g. Bianchi et al. 2005).

## 5 DISCUSSION

The detection in the *Chandra* data of two luminous ($L_{2-10\,keV} = 1.5 \times 10^{43}$ and $3.8 \times 10^{42}$ erg cm$^{-2}$ s$^{-1}$), unresolved nuclei in Mrk 463 strongly suggests that this galaxy hosts a binary AGN. While the east nucleus was already known to be a type 2 Seyfert (and this is further confirmed by our *Chandra* detection of a neutral iron line), this is the first unambiguous evidence in favour of the AGN nature of the west nucleus. These results make Mrk 463 the best *bona fide* binary AGN, only after NGC 6240, where strong neutral iron lines are detected in both nuclei. The projected separation between the two nuclei is ≃3.8 kpc, again larger only than the one measured in NGC 6240.

Fig. 4 shows the NIR spectrum of the two nuclei, using the *HST* data. In the same figure, we also plotted the *HST* NIR spectrum of two typical type 2 Seyfert galaxies taken from Alonso-Herrero et al. (2003), renormalized to the 2.1-μm flux of the two nuclei. The spectrum of Mrk 463E is reasonably well fitted by that of Mrk 573, a Compton-thick source (Guainazzi et al. 2005a), while Mrk 463W better fits that of a Compton-thin source, NGC 5252 ($N_H \simeq 5$–$7 \times 10^{22}$ cm$^{-2}$: Risaliti, Elvis & Nicastro 2002). Even if the column densities of these type 2 Seyfert galaxies do not match those of the nuclei of Mrk 463 (and, in principle, they may vary), this comparison still supports that one of the nuclei is more obscured than the other, as found in the X-rays. More direct information on the dust absorption

in Mrk 463E and its relation to the X-ray obscuration could come, in principle, from infrared (IR) spectroscopy. Indeed, the optical depth of the 3.4-μm carbonaceous dust absorption feature allowed Imanishi (2002) to estimate a dust extinction $A_V \simeq 6$–11. With the standard Galactic gas-to-dust ratio (see e.g. Maiolino et al. 2001, and references therein), this value would correspond to $N_H \simeq 2 \times 10^{22}$ cm$^2$, which is a factor of ≃35 lower than our X-ray measure. However, such an inconsistency between dust extinction and X-ray absorption is very common in AGN (Maiolino et al. 2001) and so a direct comparison between the two is difficult to interpret.

Adopting the *reddening-corrected* fluxes reported by Mazzarella & Boroson (1993), we get [O III] luminosities of $5.4 \times 10^{42}$ and $3.2 \times 10^{41}$ erg s$^{-1}$ for nucleus E and W, respectively. Therefore, with respect to the *unabsorbed* 2–10 keV X-ray luminosities derived in our *Chandra* analysis, Mrk 463W has log X/O [O III] = 1.07, which is in agreement with unobscured or Compton-thin Seyfert galaxies (e.g. Panessa et al. 2006). On the other hand, Mrk 463E has log X/O [O III] = 0.45, making it X-ray underluminous, unless it is Compton thick, but this is quite unlikely given the low EW of the iron line. Indeed, ULIRG are often found to be X-ray underluminous, but it is unclear whether it is an intrinsic property of AGN in ULIRG or it is due to the larger amount of dust available in these systems (e.g. Brandt et al. 1997; Imanishi & Terashima 2004). The interesting point here is that only one of the two active nuclei of this ULIRG is X-ray underluminous and it is the one which presents an excess with respect to the other in IR (≃30) and [O III] (≃17) emission, in comparison with the ratio of their intrinsic X-ray luminosities, which is only four. It is important to note here that almost all of the IR emission of Mrk 463E comes from the AGN, since any compact nuclear starbursts in this source are energetically insignificant, as found on the basis of the analysis of its IR spectrum (Imanishi 2002; Armus et al. 2004).

However, it must be noted that the [O III], IR and X-ray observations are not simultaneous and care must be taken when comparing them, without taking into account the source's intrinsic variability. With respect to the 1990 IR observations taken by Mazzarella et al. (1991), Mrk 463E has dimmed by 0.55 mag and Mrk 463W by 0.13 mag during the *HST* observation, taken 7 yr later. While we do not have any evidence that any of the two nuclei varied in the X-rays (we have only the *Chandra* observation analysed in this paper where the nuclei are resolved, and their combined X-ray flux is consistent with the one measured by *ASCA* and *XMM–Newton*), it is clearly possible that much (if not all) of the X-ray underluminosity of Mrk 463E may be due to the comparison of two different states of the source.

On the basis of 16 optical binary candidates, Mortlock, Webster & Francis (1999) estimated that the typical separation where the galactic nuclei become active during a merging process (the so-called 'activation radius') lies between 50 and 100 kpc. Their model also predicts that, when the merger becomes more stable, at distances around 10 kpc, the nuclei should 'turn-off' again, due to the end of the inflow of gas supplied by the merger in the previous phase. However, it is interesting to note that, with the possible exception of AM1211−465 (Jiménez-Bailón et al. 2007), all the binary AGN found in the X-rays have instead small apparent separation distances, less than ≃10 kpc.

Moreover, as already noted by Guainazzi et al. (2005b), all the AGN pairs observed so far are found to be heavily obscured in the X-rays, if not Compton thick, and the two nuclei in Mrk 463 confirm this trend. Even if based on small numbers, this result is in agreement with the idea that merging of galaxies may trigger the presence of a large amount of gas in the nuclear environment. Since obscuration

may prevent a correct classification in other bands, hard X-ray observations are indeed the most effective probes to find these elusive systems, which are expected to be abundant if our understanding of the formation and evolution of galaxies and AGN is correct.

## ACKNOWLEDGMENTS

## REFERENCES

Alonso-Herrero A., Quillen A. C., Rieke G. H., Ivanov V. D., Efstathiou A., 2003, AJ, 126, 81
Armus L. et al., 2004, ApJS, 154, 178
Arnaud K. A., 1996, in Jacoby G. H., Barnes J., eds, ASP Conf. Ser. Vol. 101, Astronomical Data Analysis Software and Systems V. Astron. Soc. Pac., San Francisco, p. 17
Awaki H., Koyama K., 1993, Adv. Space Res., 13, 221
Ballo L., Braito V., Della Ceca R., Maraschi L., Tavecchio F., Dadina M., 2004, ApJ, 600, 634
Barker E., Barker E., Barker E., Barker E., 2007, NICMOS Instrument Handbook, Version 10.0. STScI, Baltimore
Bianchi S., Matt G., Nicastro F., Porquet D., Dubau J., 2005, MNRAS, 357, 599
Bianchi S., Guainazzi M., Chiaberge M., 2006, A&A, 448, 499
Brandt W. N., Fabian A. C., Takahashi K., Fujimoto R., Yamashita A., Inoue H., Ogasaka Y., 1997, MNRAS, 290, 617
Cash W., 1976, A&A, 52, 307
Dickey J. M., Lockman F. J., 1990, ARA&A, 28, 215
Evans D. A. et al., 2007, preprint (arXiv:0712.2669)
Fruscione A., et al., 2006, in Silva D. R., Doxsey R. E., eds, Proc. SPIE Vol. 6270, Observatory Operations: Strategies, Processes, and Systems. SPIE, Bellingham, p. 60
Gabriel C. et al., 2004, in Ochsenbein F., Allen M. G., Egret D., eds, ASP Conf. Ser. Vol. 314, Astronomical Data Analysis Software and Systems (ADASS) XIII. Astron. Soc. Pac., San Francisco, p. 759
Garmire G. P., Bautz M. W., Ford P. G., Nousek J. A., Ricker G. R., 2003, in Truemper J. E., Tananbaum H. D., eds, Proc. SPIE Vol. 4851, X-Ray and Gamma-Ray Telescopes and Instruments for Astronomy. SPIE, Bellingham, p. 28
González-Martín O., Masegosa J., Márquez I., Guerrero M. A., Dultzin-Hacyan D., 2006, A&A, 460, 45
Guainazzi M., Bianchi S., 2007, MNRAS, 374, 1290
Guainazzi M., Matt G., Perola G. C., 2005a, A&A, 444, 119
Guainazzi M., Piconcelli E., Jiménez-Bailón E., Matt G., 2005b, A&A, 429, L9
Haiman Z., Quataert E., 2004, in Barger A. J., ed., Astrophys. & Space Sci. Libr. Vol. 308, Supermassive Black Holes in the Distant Universe. Kluwer, Dordrecht, p. 147
Hutchings J. B., Neff S. G., 1989, AJ, 97, 1306
Imanishi M., 2002, ApJ, 569, 44
Imanishi M., Terashima Y., 2004, AJ, 127, 758
Jiménez-Bailón E., Loiseau N., Guainazzi M., Matt G., Rosa-González D., Piconcelli E., Santos-Lleó M., 2007, A&A, 469, 881
Komossa S., 2003, in Centrella J. M., ed., AIP Conf. Ser. Vol. 686, The Astrophysics of Gravitational Wave Sources. Am. Inst. Phys., New York, p. 161
Komossa S., Burwitz V., Hasinger G., Predehl P., Kaastra J. S., Ikebe Y., 2003, ApJ, 582, L15
Landi R., Bassani L., 2001, A&A, 379, 855
Maiolino R., Marconi A., Salvati M., Risaliti G., Severgnini P., Oliva E., La Franca F., Vanzi L., 2001, A&A, 365, 28
Mazzarella J. M., Boroson T. A., 1993, ApJS, 85, 27
Mazzarella J. M., Soifer B. T., Graham J. R., Neugebauer G., Matthews K., Gaume R. A., 1991, AJ, 102, 1241
Miller J. S., Goodrich R. W., 1990, ApJ, 355, 456
Milosavljević M., Merritt D., 2001, ApJ, 563, 34
Mortlock D. J., Webster R. L., Francis P. J., 1999, MNRAS, 309, 836
Panessa F., Bassani L., Cappi M., Dadina M., Barcons X., Carrera F. J., Ho L. C., Iwasawa K., 2006, A&A, 455, 173
Piconcelli E., Jimenez-Bailón E., Guainazzi M., Schartel N., Rodríguez-Pascual P. M., Santos-Lleó M., 2004, MNRAS, 351, 161
Polletta M., Bassani L., Malaguti G., Palumbo G. G. C., Caroli E., 1996, ApJS, 106, 399
Risaliti G., Elvis M., Nicastro F., 2002, ApJ, 571, 234
Sanders D. B., Mirabel I. F., 1996, ARA&A, 34, 749
Shuder J. M., Osterbrock D. E., 1981, ApJ, 250, 55
Strüder L. et al., 2001, A&A, 365, L18
Turner M. J. L. et al., 2001, A&A, 365, L27
Ueno S., Koyama K., Awaki H., Hayashi I., Blanco P. R., 1996, PASJ, 48, 389

This paper has been typeset from a TeX/LaTeX file prepared by the author.